www.shd.org.rs

Journal of the Serbian Chemical Society

JSCS@tmf.bg.ac.yu • www.shd.org.rs/JSCS

J. Serb. Chem. Soc. 73 (11) 1083–1112 (2008)
JSCS–3789

UDC 544.4/.6.004.2+66.022.362:546.82+
621.3.032.2:544.773.42
Authors' review

AUTHORS' REVIEW

Electrocatalytic properties and stability of titanium anodes activated by the inorganic sol–gel procedure

VLADIMIR V. PANIĆ[1]*# and BRANISLAV Ž. NIKOLIĆ[2]#

[1]*ICTM – Centre for Electrochemistry, Njegoševa 12, 11000 Belgrade and* [2]*Faculty of Technology and Metallurgy, Karnegijeva 4, 11000 Belgrade, Serbia*

(Received 3 March, revised 2 September 2008)

Abstract: The properties of activated titanium anodes, RuO_2–TiO_2/Ti and RuO_2–TiO_2–IrO_2/Ti, prepared from oxide sols by the sol–gel procedure, are reviewed. RuO_2 and TiO_2 sols were synthesized by forced hydrolysis of the corresponding chlorides in acid medium. The morphology of the prepared sols was investigated by transmission electron microscopy. The chemical composition of the RuO_2 sol was determined by X-ray diffraction and thermogravimetric analysis. The loss of electrocatalytic activity of a RuO_2–TiO_2/Ti anode during an accelerated stability test was investigated by examination of the changes in the electrochemical characteristics in the potential region of the chlorine and oxygen evolution reaction, as well as on the open circuit potential. These electrochemical characteristics were investigated by cyclic voltammetry, electrochemical impedance spectroscopy and polarization measurements. The changes in electrochemical characteristics of the anode prepared by the sol–gel procedure were compared to the changes registered for an anode prepared by the traditional thermal decomposition of metal chlorides. The comparison indicated that the main cause for the activity loss of the sol–gel prepared anode was the electrochemical dissolution of RuO_2, while in the case of thermally prepared anode the loss was mainly caused by the formation of an insulating TiO_2 layer in the coating/Ti substrate interphase. The results of an accelerated stability test on RuO_2–TiO_2/Ti and RuO_2–TiO_2–IrO_2/Ti anodes showed that the ternary coating is considerably more stable than the binary one, which is the consequence of the greater stability of IrO_2 in comparison to RuO_2.

Keywords: activated titanium anodes; oxide sols; coating morphology; electrocatalytic properties; anode stability.

CONTENTS

* Corresponding author. E-mail: panic@ihtm.bg.ac.yu
# Serbian Chemical Society member.

doi: 10.2298/JSC0811083P

1. INTRODUCTION

Electrocatalytic materials based on noble metal oxides of metallic conductivity are widely used as electrodes in many fields of applied electrochemistry, such as chlorine production in the chlor-alkali and chlorate industry, processes involving oxygen generation in electroplating and metal electrowinning, as well as in cathodic protection, *etc*.[1] Most recently, these materials have been the subject of investigations in the field of supercapacitors[2–4] and fuel cells,[5,6] due to their excellent capacitive properties. Depending on the application of interest, these oxide materials are usually composed of a mixture of a noble metal oxide, such as RuO_2 or IrO_2, and an electrochemically inert, non-conductive or semi-conductive oxide (TiO_2, ZrO_2, Ta_2O_5 or Co_3O_4),[1,7–9] which stabilizes the coating and enhances the catalytic properties of the material. In the chlor-alkali industry, titanium supported RuO_2–TiO_2 coatings, known as Dimensionally Stable Anodes or Activated Titanium Anodes (ATA), are used.

In long-term electrolysis of chloride solutions a very important feature of an ATA is its service life. The anode service life and coating stability can be evaluated by an accelerated stability test (AST),[8,10] which involves the electrolysis of a dilute chloride solution at a constant high current density. The end of an anode service life, *i.e.* the loss of electrocatalytic activity, is recognized as a sudden increase in the potential. This increase in potential could be caused by 1) the growth of an insulating TiO_2 layer in the substrate/coating interface, originating from substrate corrosion, and 2) anodic dissolution of the catalytically active oxide species, RuO_2, which enriches the coating surface with TiO_2. Coating erosion can also be involved in the deactivation process.[10] The coating morphology appears to play an important role in the consideration of the cause of anode deactivation.

The anode activity for the oxygen evolution reaction, however, appears to be a key factor in the process of anode degradation.[10–13] It is known that ATA

containing iridium oxide is more stable in the electrolysis of NaCl solutions than binary RuO_2–TiO_2 coating.[12,14–16] This is due to the slower corrosion rate of IrO_2 with respect to RuO_2, since a considerable portion of the current is related to the oxygen evolution reaction.[17] For this reason, activated titanium anodes, commercially available as oxygen-evolving anodes and for cathodic protection purposes, contain iridium oxide in small amounts, in addition to ruthenium and titanium oxide.

Boodts and coworkers[8,9,18] showed that electrochemical impedance spectroscopy (EIS) provides useful information about the ATA deactivation pathway. In the case of Ti/RuO_2(x)+Co_3O_4(1–x) anodes, these authors reported the formation of a TiO_2 layer in the coating/substrate interphase as the main cause for the deactivation of anodes with low RuO_2 contents, due to high coating porosity. Anodes with a high RuO_2 content are of lower porosity, which is recognized as the cause for activity loss *via* intensive dissolution of the Ru species from the coating surface.[9]

The usual preparation method for RuO_2–TiO_2 coatings involves the process of thermal decomposition of a metal chloride mixture from organic solvents.[1,10] However, in recent years, coating preparation by the sol–gel procedure has occupied the attention of scientific workers. This is due to the possibility of preparing particles of more regular shape, size and distribution in the oxide coating.

The aim of this paper is to summarize the results of an investigation of the conditions of preparation of oxide sols and coatings on the morphology and electrochemical properties of RuO_2–TiO_2/Ti and RuO_2–TiO_2–IrO_2/Ti anodes prepared by the sol–gel procedure, especially from the standpoint of anode stability in electrolysis. The oxide sols were obtained by forced hydrolysis of an acid solution of metal chlorides at the boiling temperature. Some unique features of ATA prepared from sols obtained by the hydrolysis of alkoxides was also investtigated,[19–21] but this is not the subject of this review.

2. PHYSICO–CHEMICAL PROPERTIES OF OXIDE SOLS

The electrochemical properties of an ATA follow the basic characteristics of the oxide coating, which are influenced not only by the conditions during coating deposition (application technique and its repetition, thermal regime, coating thickness, *etc*.), but also by the physico–chemical properties of the oxide precursors. In the sol–gel procedure for coating preparation, the oxides are prepared prior to coating formation, which is the main difference with respect to thermal decomposition, when the oxides are formed *in situ* on a Ti substrate. Hence, the properties of oxide sols are reflected in the coating characteristics and, consequently, in the electrochemical properties of the ATA. The basic properties of the synthesized oxide sols and their mixture prepared for coating deposition are given in this Section, with a more detailed analysis of the ruthenium oxide sol, since this oxide is the electrocatalytically active component of the coating.

2.1. Ruthenium oxide sol

In order to check the degree of conversion in the preparation of the ruthenium oxide sol, the composition of the dry residue of the prepared sol was analyzed by energy depressive X-ray fluorescence spectroscopy (EDXRFS) and X-ray diffraction (XRD).[22] The EDXRFS spectrum is shown in Fig. 1. In addition to the high-intensity peak of ruthenium, a chlorine peak of low intensity was Registered. The appearance of the chlorine peak in the EDXRFS spectrum indicates that not all of the starting quantity of chloride precursor was converted into oxide. The XRD patterns of the dry residue of the RuO_xH_y sol, calcined at 130 °C, are shown in Fig. 2. The pattern designated as "A" was obtained for the dry residue, while "B" represents the XRD pattern of the dry residue redissolved in ethanol and dried at ambient temperature. The peaks in pattern "A" can be ascribed to crystalline ruthenium chloride, which indicates, as does the EDXRFS spectrum (Fig. 1), the incomplete conversion of the precursor. Pattern "B" in Fig. 2 indicates an amorphous structure, showing not only that ruthenium chloride does not crystallize from an ethanolic solution, but also that there is no other crystalline phase in the dry residue of the sol.

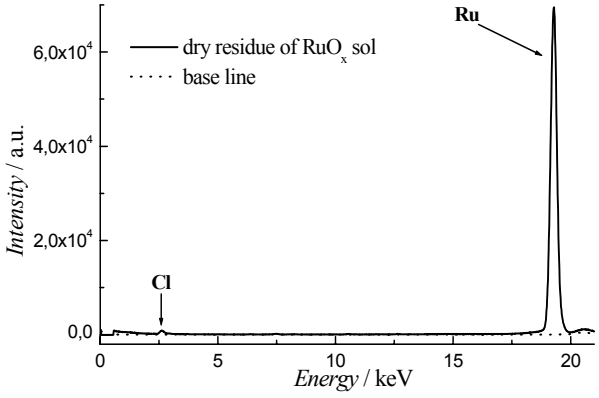

Fig. 1. EDXRFS spectrum of the solid phase of RuO_xH_y sol (Reprinted with permission of Elsevier).[22]

The forced hydrolysis process for the preparation of the sol is the time-dependent conversion of the precursor, in which some induction time for nuclei formation is necessary. For the duration of the process (ageing time), the primary nuclei grow to form the particles of the solid phase of the sol. It was shown[23,24] that the sol oxide particles grow with ageing time, which consequently influenced the electrochemical behavior of the sol–gel obtained oxide material. It was only a matter of time before all the precursor would be converted to the oxide. Bearing in mind the Ru to Cl peak intensity ratio from Fig. 1, a conversion above 95 % was achieved during the ageing time of the investigated sol, while Fig. 2 demonstrates that the formed oxide phase was amorphous.

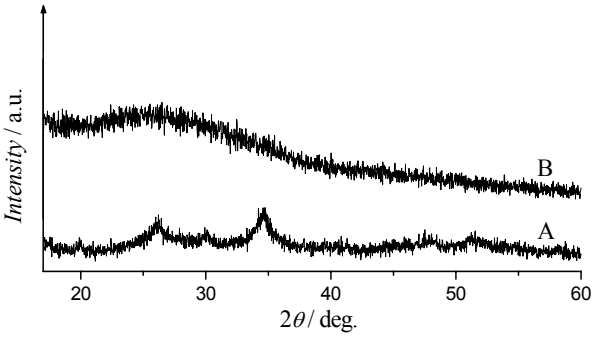

Fig. 2. XRD patterns of the solid phase of RuO_xH_y sol (A) and of RuO_xH_y sol solid phase redisolved in ethanol (B) (Reprinted with permission of Elsevier).[22]

The main feature of ruthenium oxide that defines its electrochemical properties is an optimal balance between protonic and electronic conductivity. The former increases with the water content in the hydrous oxide (RuO_xH_y), while the latter is a function of the oxide crystallinity.[22,25] Since the solid phase of the prepared sol was amorphous (Fig. 2), it should be subjected to thermal treatment in order to increase its electronic conductivity. However, the water content decreases with temperature and, consequently, so does the ability of the oxide to exchange protons with the solution. The processes that may occur during thermal treatment of the solid phase of the RuO_xH_y sol are indicated by the thermogravimetric (TG) and differential thermogravimetric (DTG) curve, which are shown in Fig. 3. The sample lost 30 % of its initial mass when the temperature was increased to around 120 °C. On the DTG curve, two minima (a and b) can be seen, indicating two processes of the release of weakly bonded water during the reversible sol–gel transition. The release of water from the hydrous oxide commences around 150 °C, and near 10 mass % was lost during a slow process accomplished around 350 °C (plateau c). In this step, one water molecule from $RuO_2{\cdot}2H_2O$ is released.[4,26] The remaining water molecule (from the monohydrate) is released at 430 °C (point d, Fig. 3), which contributes an additional 8 % mass loss. The interval d–e appears to be related to the conversion of residual chloride to oxide, since the presence chloride was registered by EDXRFS measurements (Fig. 1).

It follows from the TG measurements that the dispersed oxide retains an anhydrous nature over a wide temperature range, while the crystalline oxide structure was fully developed at the end of the processes related to the release of crystalline water, as is illustrated by the XRD pattern given in Fig. 4. These characteristics fully recommend the oxide prepared by the sol–gel process as a good protonic and electronic conductor.

Transmission electron microscopy (TEM) investigations[27] showed that the amorphous solid phase of the prepared sols consisted of spherical particles which are gathered in agglomerates. TEM images of such agglomerates are shown in Fig. 5 for sols of different ageing times. The sol with the shorter ageing time (Fig. 5a) consisted of spherical particles with a diameter of about 10 nm, while agglo-

merates with a more crystal-like structure, consisting of larger, irregularly shaped particles, were obtained at a longer ageing time (Fig. 5b).

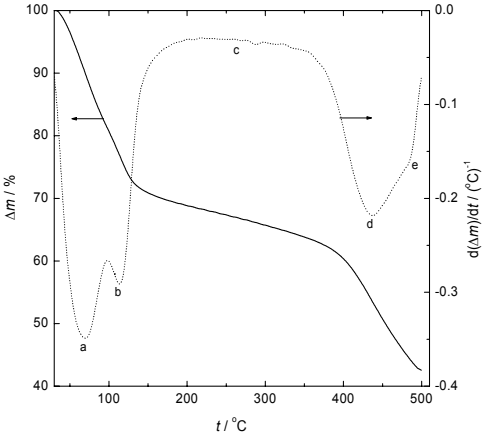

Fig. 3. TG and DTG curve registered for the solid phase of the RuO_xH_y sol.

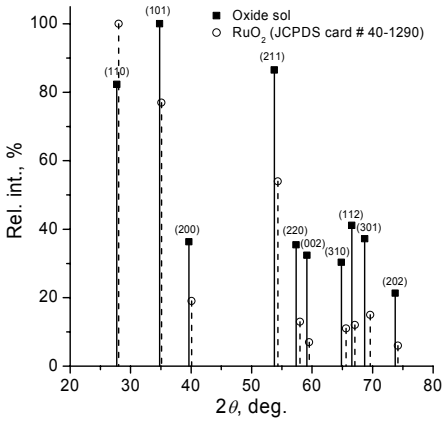

Fig. 4. XRD pattern of the solid phase of the RuO_xH_y sol annealed at 450 °C.

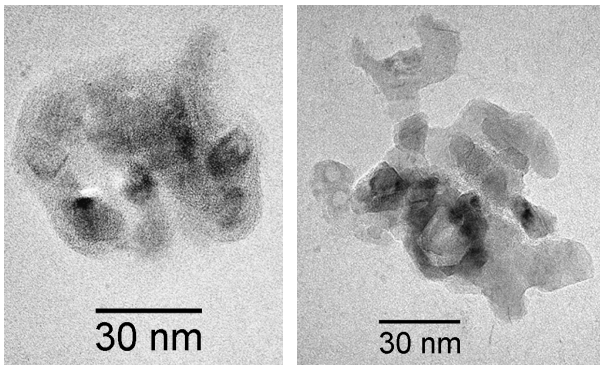

(a) (b)

Fig. 5. TEM Images of the solid phase of RuO_xH_y sol aged for 46 (a) and 94 h (b) (Reprinted with permission of Elsevier).[27]

2.2. Titanium oxide sol and sol mixture

Similar to the case of the ruthenium oxide sol, the solid phase of the prepared TiO_2 sol had an amorphous structure,[28] as it is illustrated by the XRD pattern shown in Fig. 6a, while the anatase crystal structure developed with increasing annealing temperature. In addition, the diffraction peaks become sharper with increasing temperature, which indicates an increase in the particle size.

However, in solid phase of RuO_2–TiO_2 sol mixture annealed at 450 °C, the particles of both oxides have a rutile structure, which is a usual characteristic of a thermally treated solid mixture of these oxides, regardless of the preparation procedure.[29–31]

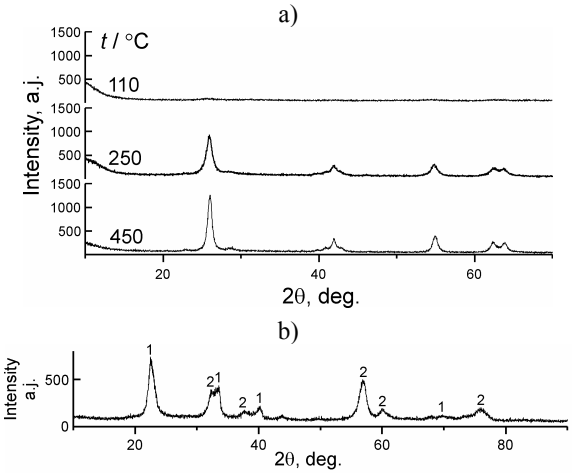

Fig. 6. XRD patterns of the solid phase of TiO_2 sol annealed at different temperatures (a) and RuO_2–TiO_2 sol mixture (b).

TEM images of differently aged TiO_2 sols are given in Fig. 7. Narrow-sized, small spherical crystallites with a diameter not larger than 5 nm form star-like agglomerates in the sol aged for the shorter time (Fig. 7a). However, with increasing ageing time, single sphere-shaped particles of a diameter around 25 nm are formed (Fig. 7b). Other authors also reported the particle size of colloidal TiO_2 in the order of nanometers.[32]

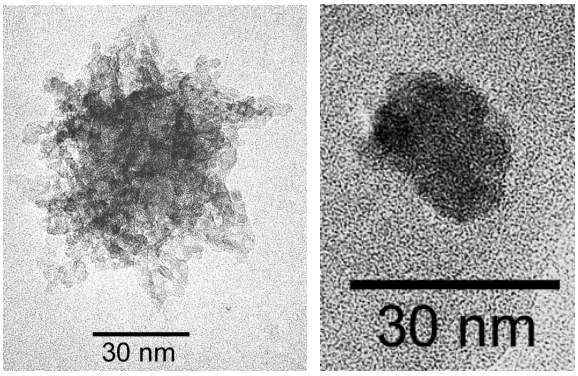

Fig. 7. TEM Images of the solid phase of TiO_2 sol aged for 15 (a) and 23 h (b) (Reprinted with permission of Elsevier).[27]

3. THE STRUCTURE AND MORPHOLOGY OF RuO_2–TiO_2 COATING

The scanning electron (SEM) microphotographs in Fig. 8 illustrate the typical appearance of the RuO_2–TiO_2 coatings prepared on titanium by the sol–gel procedure (Fig. 8a) and by *in situ* thermal decomposition of metal chlorides (Fig. 8b).[28] At the applied magnification, the sol–gel coating appears more cracked. The surface of the coatings looks like "cracked-mud" and consisted of "islands" (surface area ≈ 60 μm^2) separated by cracks, which are wider on sol–gel coating surface. The appearance of cracks also suggests that the islands in the sol–gel coating are made of distinct layers, while "thermal" coating appears smoother.

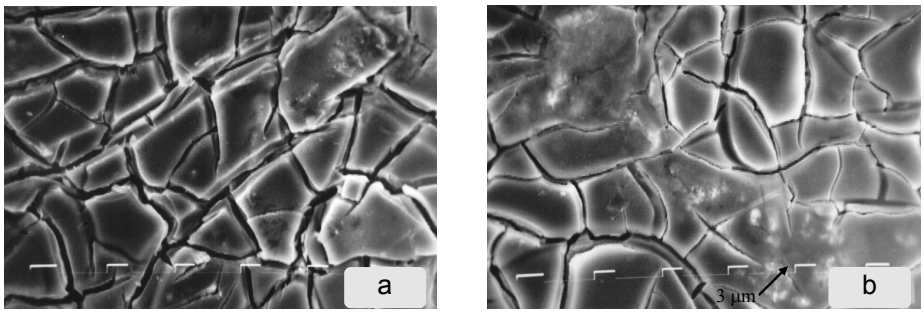

Fig. 8. Typical SEM microphotographs of RuO_2–TiO_2 coatings obtained by: a) the sol–gel procedure and b) thermal decomposition (Reprinted with permission of Elsevier).[28]

The essential difference in morphology between the sol–gel processed and thermally prepared RuO_2–TiO_2 coating is registered on the nano-scale.[27,28] The typical surface appearance on the nano-scale of the coatings prepared by the sol–gel procedure and thermal decomposition is given by the scanning tunneling microscopy (STM) 3D surface nanophotographs (scan size: 50 nm×50 nm) given in Fig. 9.

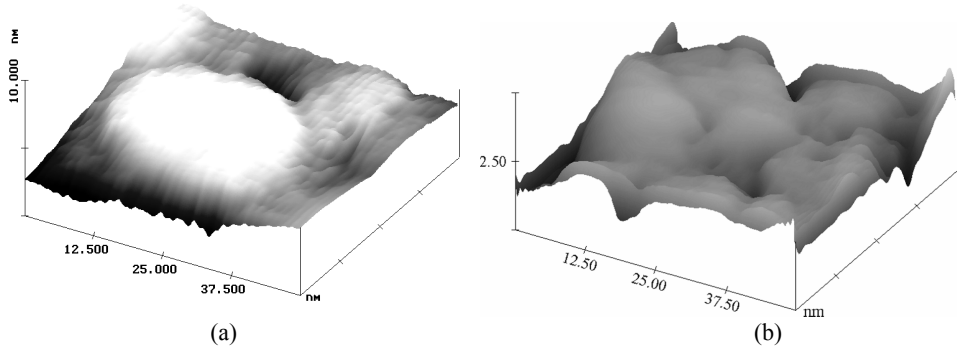

(a) (b)

Fig. 9. Typical STM microphotographs of the RuO_2–TiO_2 coatings obtained by: a) the sol–gel procedure and b) thermal decomposition (Reprinted with permission of Elsevier).[27,28]

It can be seen that the nano-roughness is more pronounced for the surface of sol–gel prepared coating (Fig. 9a). The average difference between real and geometric surface area, according to the STM data, was found to be two-fold greater for the sol–gel coating. The sharp nano-spots, which are ubiquitous on the surface of sol–gel coating, cannot be seen on the thermal one. It could be assumed that these surface characteristics are the result of the more defined oxide particles formed in the case of the sol–gel coating. The size of the spots is very similar to the RuO_2 particle size registered by TEM (Fig. 5a). Another important difference is the appearance of bright areas on the sol–gel coating, having a size of about 30 nm (Fig. 9a). Taking into account the size of the TiO_2 particles observed in the TEM image of the TiO_2 sol (Fig. 7b), being close to 25 nm, the conclusion appears to be that the bright areas in Fig. 9a are the large grains of TiO_2. It seems that small

the RuO_2 particles are on the top of and around each TiO_2 grain in the sol–gel prepared coating.[27]

4. CAPACITIVE ABILITY OF ACTIVATED TITANIUM ANODES AS THE FUNCTION OF THE PROPERTIES OF OXIDE SOLS

The pronounced capacitive ability of noble metal oxides is the consequence of pseudocapacitive behavior due to solid-state surface redox transitions of the metal ions, which is closely related to the oxide protonic conductivity.[1,2,33] Generally, proton-assisted redox transitions are written as follows:[33]

$$RuO_x(OH)_y + \delta H^+ + \delta e^- \rightarrow RuO_{x-\delta}(OH)_{y+\delta}, \quad 0 \leq \delta \leq x \qquad (1)$$

The transition reactions can be diffusion-controlled to different degrees by the proton injection/ejection process, depending on the coating porosity. On the other hand, the capacitance depends on the surface area. These features are directly influenced by the coating morphology, preparation procedure and oxide particle size,[19,20,23,27,34] which results in the capacitance being dependent on the rate of the charging/discharging process.

4.1. Preparation procedure, coating composition and capacitive response

The cyclic voltammograms (CV) of a sol–gel and a thermally prepared ATA recorded in acid solution are shown in Fig. 10. The registered CV shape is usual for RuO_2-based electrodes,[2,23,33] with a broad peak in the potential region from 0.20 to 0.50 V, which is related to the redox transition presented by Eq. (1). The voltammetric current densities recorded for the sol–gel prepared anode are larger than those recorded for thermally prepared one. This indicates the larger electrochemically active surface area[7] of the sol–gel prepared anode, due to the larger real surface area and greater RuO_2 content in the surface layer of the sol–gel prepared coating.[31] Using the approach of Da Silva *et al*.[35] for the values of the morphology factor, 0.50 and 0.52 are obtained for sol–gel and thermally prepared coating, respectively. These similar values indicate the similar contribution of inner coating surfaces to the overall coating capacitance, due to similar porosity of the coatings.[36]

The addition of a small amount of iridium oxide (10 mol %), either as *in situ* converted chloride or as previously prepared sol, into the sol–gel prepared RuO_2–TiO_2 coating results in an increase in the capacitive ability.[37] The voltammograms of ternary and binary coating registered in acid solution are shown in Fig. 11. The increase in the voltammetric currents were more pronounced at potentials positive to 0.40 V due to the imposed contribution of redox transitions of iridium species. If IrO_2 was applied from the sol, the effects were more pronounced.

4.2. The voltammetric charge and properties of the oxide sols

The dependence of coating capacitive ability on the ageing time, t_{ag}, (*i.e.* oxide particle size, Section 2) of the oxide sols was analyzed through the values of voltammetric charges.[23]

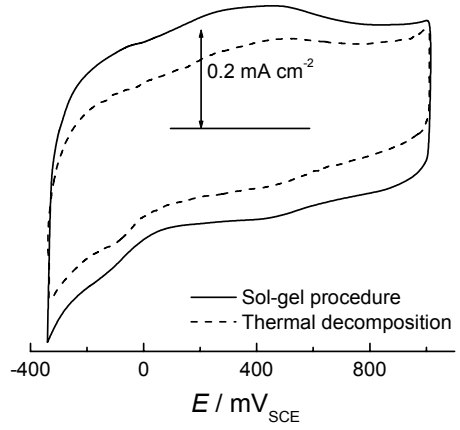

Fig. 10. Cyclic voltammograms of the RuO_2–$–TiO_2$/Ti electrodes prepared by the sol–gel and thermal procedure. Scan rate: 20 mV s^{-1}. Electrolyte: 1.0 mol dm^{-3} $HClO_4$.

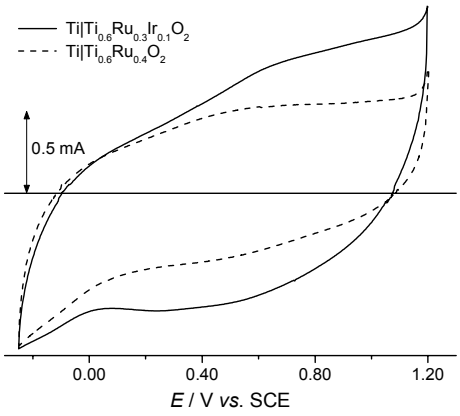

Fig. 11. Cyclic voltammograms of the RuO_2–$–TiO_2$–IrO_2/Ti and RuO_2–TiO_2/Ti electrodes prepared by the sol–gel procedure. Scan rate: 20 mV s^{-1}. Electrolyte: 1.0 mol dm^{-3} H_2SO_4.

The total charge, q^*_{tot}, related to the whole electrochemical surface area of the coating, could be separated into two components: the first, q^*_{out}, related to the "outer" parts of the coating, which are directly exposed to the electrolyte, and the second, q^*_{in}, related to the "inner" parts of the coating, which are hidden in loose grain boundaries, pores and cracks. The total charge, as well as its components, can be evaluated from the dependencies:

$$q^*(v) = q^*_{out} + kv^{-1/2} \quad (2)$$

$$q^*(v)^{-1} = (q^*_{tot})^{-1} + k'v^{1/2} \quad (3)$$

and

$$q^*_{tot} = q^*_{in} + q^*_{out} \quad (4)$$

where q^* is the charge obtained by integration of anodic part of the voltammetric curve at a given sweep rate v; k and k' are constants.

The values of the voltammetric charges obtained using Eqs. (2)–(4) as functions of the aging time of the RuO_2 and TiO_2 sol are shown in Fig. 12. For ageing times of the RuO_2 sol shorter than about 40 h, all three kinds of charge increase with increasing ageing time (Fig. 12a). After 40 h of ageing, the charges decrease with ageing time. Since these changes are seen for all three kinds of charge, it could be concluded that the particles from the RuO_2 sols of different ageing result in similar morphological changes in the outer surface of the coating as well as in its inner parts. The largest charge related to an anode obtained with a RuO_2 sol aged for about 40 h suggests that the solid phase of this sol had the largest ratio of small RuO_2 particles.[38] Smaller charge values related to anodes obtained with RuO_2 sols aged for times shorter than 40 h indicate that the particles of these sols were larger than those from the sol aged for about 40 h. Taking into account the fact that complete sol particle formation in the forced hydrolysis procedure requires some critical time,[39] it is to be expected that the formation of the RuO_2 sol particles is not completed in ageing times shorter than 40 h. In addition, it is assumed that the large RuO_2 particles in the coatings obtained with sols aged for times shorter than 40 h originate from the thermal decomposition of the residual $RuCl_3$ which had not been converted to RuO_2 by forced hydrolysis. The ratio of larger RuO_2 particles dispersed in the solid phase increased for ageing longer than 40 h, which causes a decrease of the charge related to the anodes obtained with these dispersions.

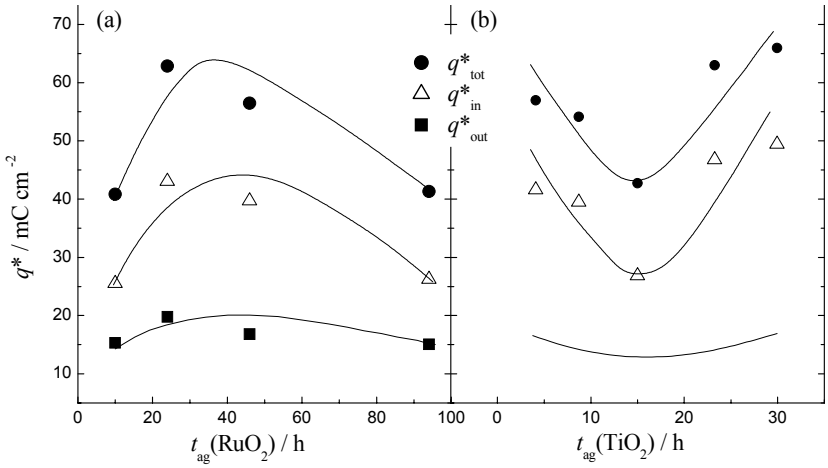

Fig. 12. The charge densities related to the total, inner and outer electrochemical surface area of the anode coating as functions of the ageing time of RuO_2 (a) and TiO_2 (b) sols used for the preparation of the coatings (Reprinted with permission of Elsevier).[23]

The influence of the ageing time of TiO_2 sol on the charges of the prepared anodes is shown in Fig. 12b. The values of all three types of charges decreased with increasing aging time of TiO_2 sol up to 15 h and then increased, although

the changes in q^*_{out} were less pronounced. Since the ratio of large sol particles increases with increasing ageing time, it could be concluded that the growth of TiO_2 particles during the ageing of TiO_2 sols causes the enlargement of the ESA of the coating obtained from these sols. For ageing times shorter than 15 h, similar to the case of the aging of the RuO_2 sol, particle formation was not completed and the ratio of large TiO_2 particles resulting from the thermal decomposition of residual $TiCl_3$ was high. Accordingly, the anode obtained with TiO_2 sol aged 15 h had the smallest ESA, which means that the solid phase of this sol contained the highest ratio of small TiO_2 particles.

The observed changes in ESA with ageing time of the TiO_2 sol are clearly reflected from the changes in the difference between the real and apparent surface area (*SAD*) obtained from STM measurements.[27] The changes in macro-, micro- and nano-roughness with $t_{ag}(TiO_2)$ are shown in Fig. 13. While the macroscopic roughness (880 nm × 880 nm) does not depend on $t_{ag}(TiO_2)$, the shapes of the micro- (250 nm × 250 nm) and nano-roughness (50 nm × 50 nm) dependencies are quite similar to the dependencies presented in Fig. 12b.

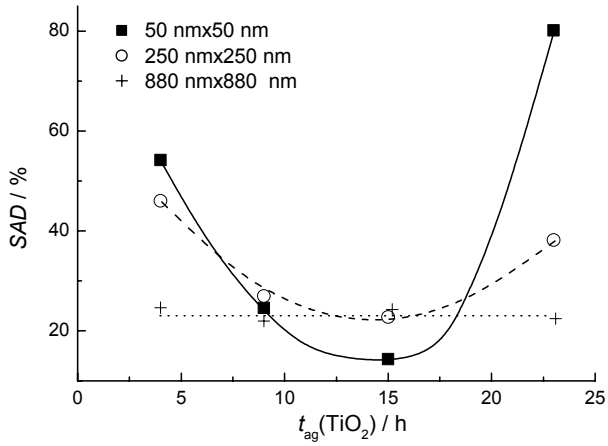

Fig. 13. Difference between real and apparent surface area (*SAD*, surface area difference) of RuO_2–TiO_2 coating prepared by the sol–gel procedure from differently aged TiO_2 sols. The ageing time of the RuO_2 sol was fixed at 46 h.

5. THE ACTIVITY FOR Cl_2 AND O_2 EVOLUTION REACTION

Tafel plots of the ATA prepared by the sol–gel procedure and thermal decomposition in the chlorine evolution reaction, as an indication of their electrocatalytic properties, are given in Fig. 14. The slope values close to 40 mV for both the sol–gel prepared and the thermally formed coatings correspond to the known mechanism of the chlorine evolution reaction on RuO_2-type coatings.[1,10,23] Higher current densities were registered for the sol–gel prepared anode. Normalized data (given by symbols ◇ and ○ for sol–gel and thermally prepared anode, respecttively) was obtained by dividing the measured currents densities by the corresponding q^*_{tot} values. Since the geometric factor (surface area) is eliminated in this way, the normalized data give the real catalytic activity of RuO_2.[33,40] The

normalized catalytic activity is practically the same for the sol–gel and the thermally formed anode. This leads to the conclusion that the difference in real surface areas of the sol–gel and thermally prepared anode, influenced by coating morphology, is the key parameter that causes the difference in their electrochemical behavior.[41]

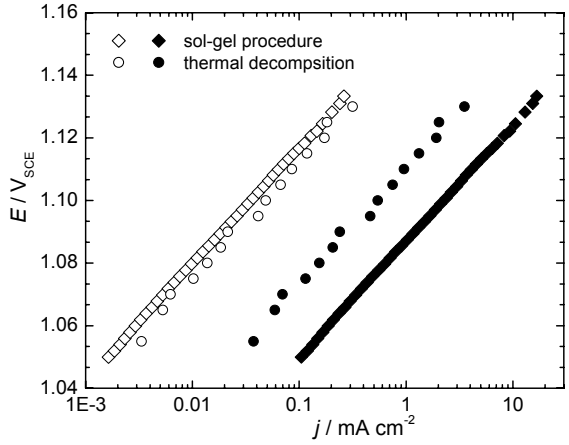

Fig. 14. The apparent (●,◆) and normalized (○,◇) Tafel plots of the sol–gel and thermally prepared anode. Electrolyte: 5 mol dm^{-3} NaCl, pH 2 (Reprinted with permission of Taylor & Francis).[41]

The normalized activities of the sol–gel prepared anode, however, show a dependence on the ageing time of oxide sol.[23] The dependences of the normalized values of the current densities on ageing time of the RuO_2 and TiO_2 sol are shown in Fig. 15. The changes of electrocatalytic activity with oxide particle size are similar to those obtained for ESA with oxide particle size (Fig. 12). The highest activities were achieved for anodes obtained with the RuO_2 sol aged for about 40 h and the TiO_2 sol aged for 30 h. The anode obtained with TiO_2 sol aged for 23 h had the smallest activity. The dependence of the anode electrocatalytic activity on the aging time was more pronounced in the case of the TiO_2 sol than in the case of the RuO_2 sol. The observed activity effects are probably due to the appearance of different states of the active sites, caused by different TiO_2 particle sizes and the revealing effect of TiO_2. A similar effect of the appearance of "new" active sites was also observed in the case of RuO_2 coatings obtained with rare earth oxides.[42,43] In the case of the RuO_2–TiO_2 binary oxide, the appearance of "new" active sites could be the consequence of different physical interaction between these two oxides, which depends on the TiO_2 particle size.

The ternary coating, obtained by the addition of a small amount of IrO_2, showed no significant difference in activity for chlorine and oxygen evolution with respect to the binary coating.[37] The Tafel plots given in Fig. 16 show that the polarization curves have the usual values of the Tafel slopes and negligibly higher activity of binary coating for chlorine evolution.

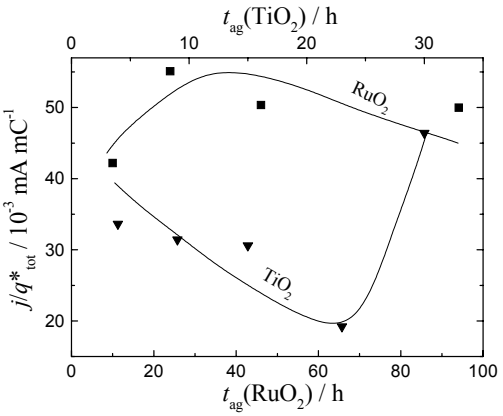

Fig. 15. Normalized activity of the sol–gel coatings at a potential of 1.10 V as a function of the ageing time of the RuO_2 and TiO_2 sols used for coating preparation (Reprinted with permission of Elsevier).[23]

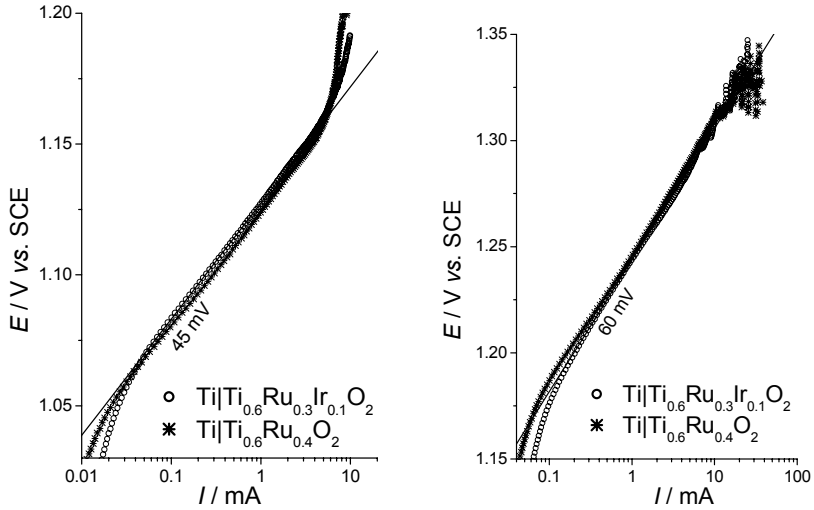

(a) (b)

Fig. 16. Tafel plots for the chlorine (a) and oxygen (b) evolution reaction registered for binary and ternary coating prepared by the sol–gel procedure.

6. THE STABILITY IN Cl_2 AND O_2 ELECTROLYSIS

The main industrial application of ATA is in long-term electrolysis of acid or neutral solutions, both chloride-containing and not. The anode wears during the electrolysis and finally ends its operation.[10–13] The dissolution of electrochemically active coating component (*e.g.* RuO_2 and IrO_2) and coating enrichment in insulating and inactive TiO_2 are recognized as the causes of the wearing process.[11] In addition to dissolution, the TiO_2 content can increase due to anodic oxidation of the Ti substrate, forming an insulating coating/substrate interlayer.[10] In this Section, the stability of binary and ternary coatings will be analyzed and com-

pared to the stability of traditional binary thermal coatings. The possible mechanism of anode wearing and the loss of electrocatalytic activity will be given.

The time dependence of the relative electrode potential, as the result of an accelerated corrosion test, for anodes prepared by the sol–gel and thermal procedure is shown in Fig. 17. The sol–gel prepared anodes with a binary coating showed considerably longer lifetimes than the thermal ones. The causes for the greater stability could be either the larger surface area of the sol–gel prepared anode or different mechanisms of the loss of catalytic activity or both. The morphology of the coating can influence any characteristic step in the mechanism. According to the STM data (Fig. 9), it is believed that the oxide particle size and distribution is more regular in the case of the sol–gel procedure then in the case of the thermal one, which produces a larger surface area and, consequently, the real current density of Ru dissolution on a sol–gel anode is smaller. In the same manner, the structure of the catalytic coating of a sol–gel prepared anode could be more homogeneous and the penetration of the electrolyte towards the titanium substrate thus hindered, which, besides the smaller current density, makes the chance for nonconductive intermediate TiO_2 layer formation smaller as compared to a thermally prepared anode.[28]

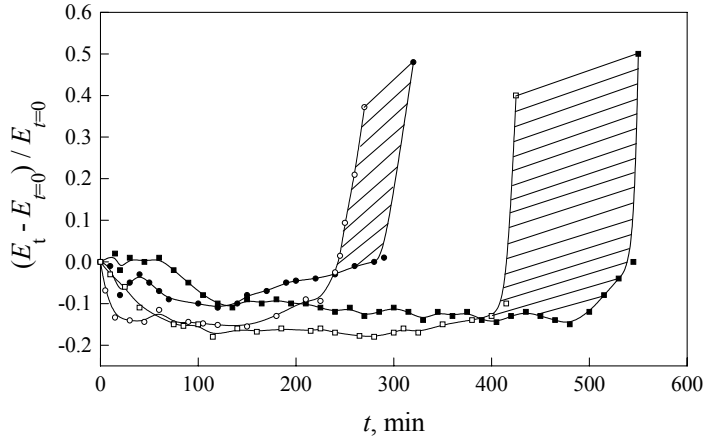

Fig. 17. The results of accelerated stability test: (–○–) thermally and (–□–) sol–gel prepared anodes with the shortest lifetime; (–●–) thermally and (–■–) sol-gel prepared anodes with the longest lifetime (the lifetimes for other samples of both types of anodes lay in the shaded areas). Electrolyte: 0.50 M NaCl, pH 2. Temperature: 35 °C, j = 2.0 A cm^{-2}. Total amount of oxide: 2.0 mg cm^{-2}. (Reprinted with permission of Elsevier).[28]

The stability of binary sol–gel coating can be controlled by changing the properties of the oxide sols. The influence of the ageing time of RuO_2 and TiO_2 sols on the stability of obtained anodes is presented in Fig. 18. The anode stability was the greatest when the RuO_2 sol was aged for about 40 h, *i.e.* when the ratio of small RuO_2 particles in RuO_2 sol was the highest. The change in stability

can be discussed in accordance to the changes of coating ESA with ageing of RuO_2 sol (Fig. 12). The rate of loss of activity *via* Ru dissolution decreases as the ESA increases or as the RuO_2 particle size decreases. In addition, the real current density of Ru dissolution is distributed more regularly if the RuO_2 particles are smaller, because they are more regularly packed throughout the bulk of the coating. Summarizing the above considerations, the anode with highest ratio of small RuO_2 particles, obtained with the RuO_2 sol aged for about 40 h, was the most stable due to it having the largest ESA.

The anode was more stable if the ageing time of the TiO_2 sol increased or if the TiO_2 particle size increased, due to similar consideration as in the case of the variation of the ageing time of the RuO_2 sol.

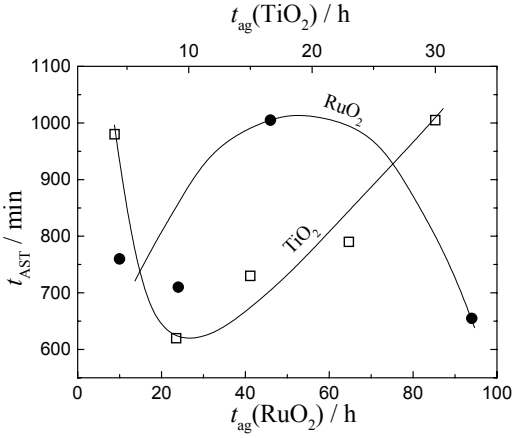

Fig. 18. The dependencies of RuO_2–TiO_2/Ti anode durability obtained by an accelerated stability test (AST) (electrolyte: 0.50 M NaCl, pH 2, j = 2.0 A cm^{-2}, 33 °C) on the ageing time of RuO_2 and TiO_2 sols used for the anode preparation. (Reprinted with permission of Elsevier).[23]

6.1. The mechanism of anode deactivation

In order to gain further insight into the wear mechanism, anodes with thin sol–gel or thermally prepared coatings were investigated in more detail when approaching the end of their service life.[36] The time dependences of the anode potential and the appropriate differential curves for the anodes with thin coatings prepared by sol–gel and thermal procedure are shown in Fig. 19. The current density was lower than in the tests shown in Figs. 17 and 18, in order to obtain well resolved wear steps at the end of the service life of the anodes. Two distinct regions in the plots in Fig. 19 can be seen. In the period below 29 h, the anode operation is stable. The potential has a stable value not exceeding the initial value by more than 20 %. The potential increased slightly during the first few hours of the AST, which could be the consequence of the presence of evolved gas bubbles at the anode surface. Tumultuous anode disordering is observed after 29 h as a continuous increase in the potential. The service lives of both the sol–gel and thermally prepared anode were practically the same, which was not the case with thick coatings, when the sol–gel procedure provided coatings with a longer service life (Fig. 17). The increase in potential and the rate of increase in potential were quite

similar for both the sol–gel and thermally prepared anode up to 30.7 h of AST, but a difference in the change of potential values was seen after this time. The rate of increase in potential of the thermally prepared anode was constant, being around 0.1 V min^{-1}, while the rate of the change in potential values of the sol–gel prepared anode considerably increased. These observations at the end of anode service life indicate a different deactivation mechanism for the anodes prepared by the sol–gel and thermal procedure.

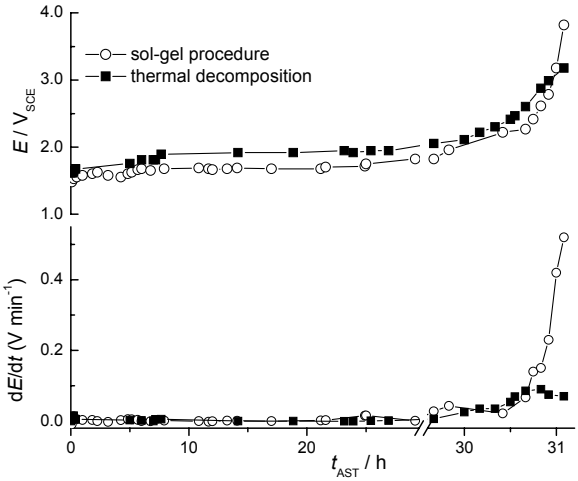

Fig. 19. The change of anode potential as a function of time during AST for RuO_2–TiO_2/Ti anodes prepared by the sol–gel procedure and thermal decomposition. Electrolyte: 0.50 mol dm^{-3} NaCl, pH 2, 25 °C. Current density: 700 mA cm^{-2}. (Reprinted with permission of Elsevier).[36]

6.2. The changes in electrochemically active surface area during deactivation

The changes in electrochemically active surface area of the coatings during AST are presented by the data given in Fig. 20, which shows the changes in apparent capacitances, calculated for a 1 V potential window from the cyclic voltammograms registered during AST and normalized to the apparent electrode surface area. After a period of 29.7 h of AST, the capacitance of both the sol–gel and thermally prepared anode increased in comparison to the capacitance Registered before AST. This could be explained by an increase in the real surface area of the coating. As the Ru species from the coating surface undergo dissolution during AST, the coating roughness increased, while the orifices of pores and cracks became wider. This makes the inner parts of the coating more accessible to the electrolyte. Assuming that the thermally prepared coating consisted of larger particles than the coating prepared by the sol–gel procedure,[44] the increase in coating roughness is more pronounced and the electrolyte penetrates more easily to the bulk of thermally prepared coating. This should lead to a more pronounced increase in capacitance of the thermally prepared coating for t_{AST} = 29.7 h. For AST times between 29.7 and 30.5 h, the capacitance decreased. During this short period, the intensive dissolution of Ru species leads to a considerable decrease in the number of active sites in the coating, *i.e.* electrochemically active surface area of the coating.

The essential difference in the C–t_{AST} dependencies for the sol–gel and thermally prepared anode appeared for t_{AST} larger than 30.5 h. While the capacitance of the sol–gel prepared anode continuously decreased going towards the end of its service life, the thermally prepared anode maintained the capacitance value registered for $t_{AST} \approx 30.5$ h. In this period, more reliable capacitance data for the thermally prepared anode are obtained by impedance measurements (see Section 6.4).

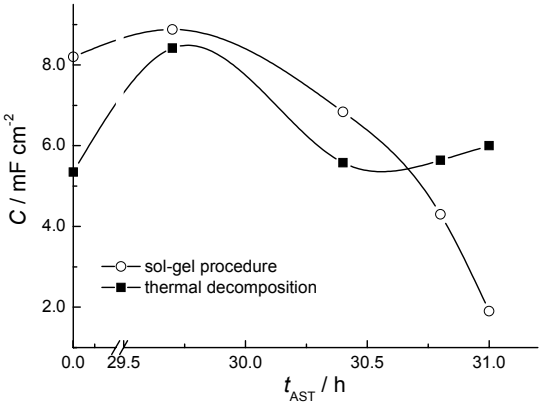

Fig. 20. The capacitances per apparent surface area of the anodes prepared by the sol–gel (○) and thermal procedure (■) calculated from cyclic the voltammograms recorded in 1.0 mol dm^{-3} $HClO_4$ during AST (Reprinted with permission of Elsevier).[36]

6.3. The loss of electrocatalytic activity

Polarization measurements in both NaCl and $HClO_4$ solution showed that the time of subjection of an anode to AST influenced the current, the Tafel slope and the potential range of the Tafel dependences. The apparent current density of chlorine evolution at a potential of 1.15 V, as well as the Tafel slope obtained from E–log j dependencies corrected for pseudo-ohmic resistance, and the values used for this correction are shown as function of t_{AST} in Fig. 21. Generally, the current decreased with t_{AST}, while the Tafel slope and pseudo-ohmic resistance increased for both the sol–gel and thermally prepared anode, as a result of anode deactivation. Similar dependencies were obtained for oxygen evolution from an $HClO_4$ solution.

As can be seen, the current–AST time dependences (Fig. 21a) are similar to the anodic C–t_{AST} dependencies (Fig. 20). There was an initial increase in the current density with t_{AST}, followed by a decrease as the anodes approach the end of their service life. The initial increase was more pronounced for the sol–gel prepared anode than for the thermally prepared one, which is opposite to the change in capacitance. In addition, an almost three times higher current density was registered before AST for the anode prepared by thermal decomposition. This behavior could be due to the larger number of active sites that participate in the O_2/Cl_2 evolution reaction,[45] owing to the wider cracks and pores of the thermally prepared anode.

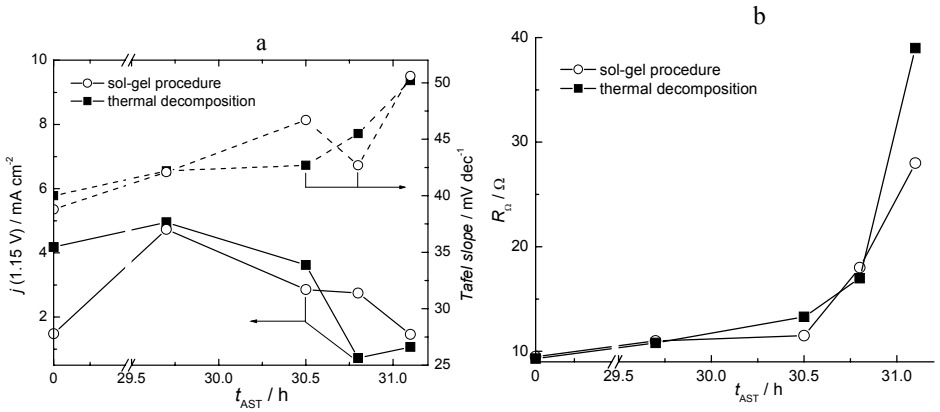

Fig. 21. The changes in current density at potential 1.15 V_{SCE} and Tafel slope registered by polarization measurements in 0.50 mol dm^{-3} NaCl, pH 2, (a) and pseudo-ohmic resistance used for correction of Tafel dependencies (b), during the accelerated stability test. (Reprinted with permission of Elsevier).[36]

According to the theory of porous electrodes,[45] the overvoltage exponentially decreases going from the surface toward the bulk of the porous layer. The decreasing function depends on the layer morphology. Considering layers of the same thickness but of different porosity and/or tortuosity, active sites at different distances from the surface are at different overvoltage values. The higher current densities registered for the thermally prepared anode before AST means that a larger number of inner active sites contribute to the reaction than in the case of the sol–gel prepared anode. Since the thermally prepared anode had wider pores and cracks, there is a better access of the electrolyte to the inner active sites of the thermally prepared anode and an easier release of gas bubbles from the pores and cracks. With the sol–gel prepared anode, only the active sites situated at the surface of the coating participate in reaction because of the narrow pores and cracks.

The increase in current density registered for both the sol–gel and thermally prepared anode for t_{AST} = 29.7 h (Fig. 21a) is due to an increase in the coating roughness. This initial period should be thus considered as an "opening of the inner coating structure". Once the inner coating structure is "opened", progressive dissolution of the active Ru species occurs, resulting in a decrease in the total number of active sites. For t_{AST} between 30.5 and 30.8 h, the current density for the thermally prepared anode decreased considerably, while the sol–gel prepared anode maintained the activity registered for t_{AST} = 30.5 h. This indicates a larger inner electrochemically active surface area of the sol–gel prepared coating, due to the more homogeneously dispersed oxide catalyst within the coating bulk.

As can be seen in Fig. 21b, the deactivation process during AST was also followed by a continuous increase in the pseudo-ohmic resistance within the coating. Similar values of the pseudo-ohmic resistance were obtained for both the

sol–gel and thermally prepared anode during AST, except at the end of the service life. For AST times longer than 30.7 h, a more pronounced increase in the pseudo-ohmic resistance was registered for the thermally than for the sol–gel prepared anode.

6.4. Impedance characteristics during the deactivation

The complex plane plots of the EIS data registered in 1 mol dm^{-3} $HClO_4$ during AST for the sol–gel and thermally prepared anode are shown in Fig. 22 and Fig. 23, respectively. The results of a fitting procedure are presented by the lines.

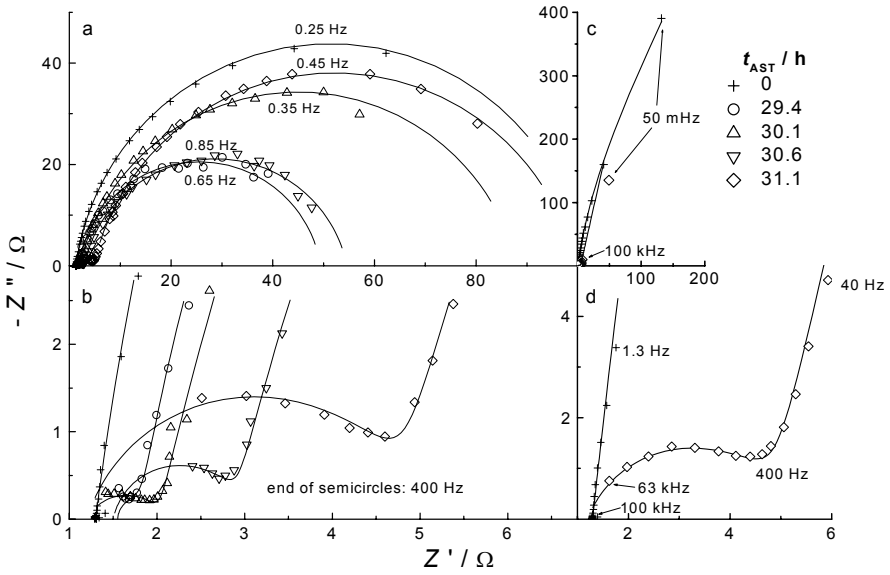

Fig. 22. Complex plane plots of the EIS data registered for the sol–gel prepared anode in 1.0 mol dm^{-3} $HClO_4$ at a potential of 1.25 V_{SCE} (a and b) during AST and at 0.50 V_{SCE} (c and d) before (0 h) and after (31.1 h) of AST; a,c – whole frequency range and b,d – high frequency range. (Reprinted with permission of Elsevier).[36]

A semicircle at low frequencies was registered at a potential of 1.25 V, which is associated with charge transfer in the oxygen evolution reaction (Figs. 22a and 23a), while a capacitive-like response was seen at a potential of 0.50 V (Figs. 22c and 23c). As can be seen in Figs. 22b and 23b, the continuous deactivation of both the sol–gel and thermally prepared anode during AST is manifested by the appearance of a growing semicircle in the high-frequency domain of the complex plane plots. In addition, there are simultaneous changes in the diameter of the low-frequency semicircle (Figs. 22a and 23a). The appearance of a high--frequency semicircle and the difference in the EIS data from the low-frequency domain, caused by anode deactivation, was also registered at 0.50 V. The similar values of the diameters of the high-frequency semicircle registered at different

potentials (1.25 and 0.50 V) after the same AST time (31.1 h) mean that the corresponding resistance was not due to a charge transfer process. Although the changes in EIS behavior during AST are similar for both the sol–gel and thermally prepared anode, the difference in characteristics of the registered semicircles as well as in the capacitive behavior at 0.50 V is obvious.

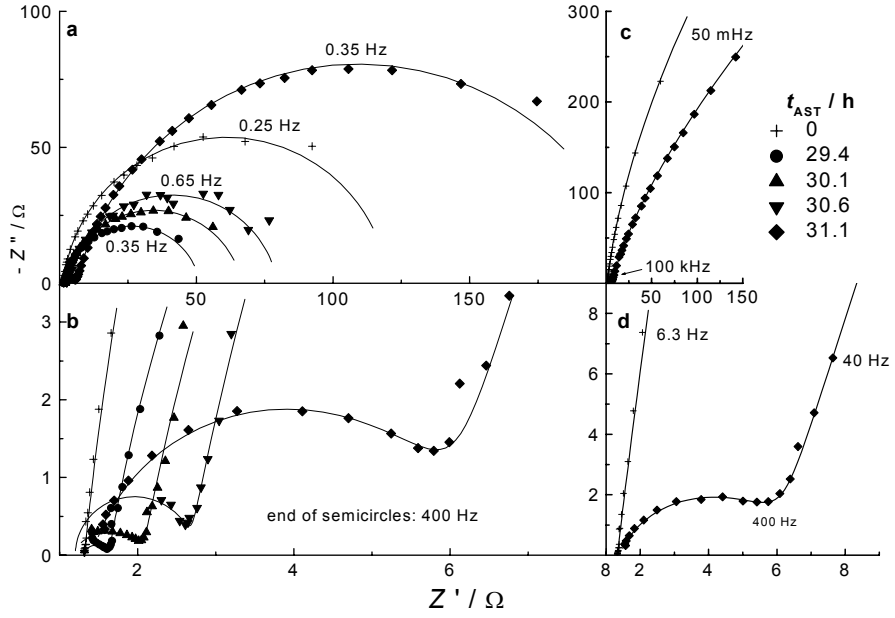

Fig. 23. Complex plane plots of EIS data registered for the thermally prepared anode in 1.0 mol dm^{-3} $HClO_4$ at a potential of 1.25 V_{SCE} (a and b) during AST and at 0.50 V_{SCE} (c and d) before (0 h) and after (31.1 h) AST; a,c – whole frequency range and b,d – high frequency range. (Reprinted with permission of Elsevier).[36]

The complex plane plots of EIS data registered in 0.50 mol dm^{-3} NaCl, pH 2, at a potential of 1.15 V, before and after AST for both the sol–gel and thermally prepared anode are shown in Fig. 24. A semicircle is seen before AST in the high-frequency domain, which relates to charge transfer in the chlorine evolution reaction. At lower frequencies, a straight line follows the semicircle. By fitting procedure using the Randles–Shevchik equivalent circuit with a constant phase element instead of a Warburg element, the values of the *n* parameter between 0.49 and 0.55 were obtained. This indicates diffusion limitations to the charge transfer process.

The diameter of the semicircle registered before AST for the thermally prepared anode was larger in comparison to that for the sol–gel prepared anode (Fig. 24). This indicates the greater activity of the sol–gel prepared anode for the chlorine evolution reaction, contrary to the higher apparent current density registered for the thermally prepared anode by polarization measurements (Fig. 21). This

observation supports the conclusion that the higher current densities of the thermally prepared anode were due to the wider pores and cracks of this anode.

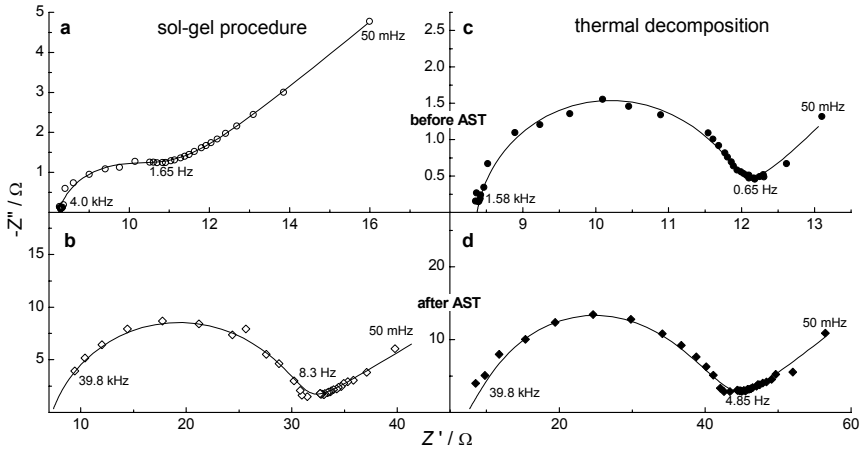

Fig. 24. Complex plane plots of EIS data registered for the sol–gel (a and b) and thermally (c and d) prepared anode in 0.50 mol dm^{-3} NaCl, pH 2, at the potential 1.15 V_{SCE} before (0 h) and after (31.1 h) AST. (Reprinted with permission of Elsevier).[36]

As a consequence of anode deactivation, semicircles of considerably larger diameters in comparison to those registered before AST are seen in Fig. 24. In addition, the semicircles are shifted towards higher frequencies. Semicircles of similar diameters were also registered at 0.50 V in NaCl solution after AST (not shown), which implies that the semicircle related to charge transfer and that appearing as a result of anode deactivation are overlapped. In NaCl solution, the resistance related to the high-frequency semicircle after AST is an order of magnitude greater than in $HClO_4$ solution (Figs. 22d and 23d), which suggests that this resistance refers to the electrolyte in the pores (pore resistance, R_p) of an insulating layer formed on the coating surface during anode deactivation. The ohmic resistance, R_Ω is also an order of magnitude larger in NaCl solution (*e.g.*, Figs. 22b and 24b). The sum of R_Ω and R_p, as obtained by a fitting procedure[46] of the EIS data registered in NaCl solution, for the sol–gel and thermally prepared anode after AST is 27 and 41 Ω, respectively. These values are very similar to the values of the pseudo-ohmic resistance used for the correction of the Tafel plots (Fig. 21b), which confirms that Rp corresponds to the ohmic resistance of the electrolyte.

The part of the complex plane plots in Fig. 24 related to the diffusion limitations differs for the anodes prepared by the sol–gel procedure and thermal decomposition, as well as for the anode before and after AST. This means that the transport of the reacting species involves diffusion through the electrolyte in the coating pores. The diffusion limitations were more pronounced for the sol–gel prepared anode than for the thermally prepared one, which indicates the wider

pores and cracks of the latter. Due to anode deactivation, the diffusion tails for both the sol–gel and thermally prepared anode commence at higher frequencies if compared to the tails before AST, which indicates that the reacting species reach active sites situated deeper in the coating.

6.4.1. Changes in the capacitive behavior

The best description of the impedance behavior of the active and deactivated coatings at 0.50 V (Figs. 22 and 23) was obtained using a transmission-line equivalent electrical circuit (EEC).[2] This kind of circuit indicates the capacitive responses of active sites situated on the outer and inner active surface, similarly to Eqs. (2) and (3). For the active (before AST) sol–gel and thermally prepared anode, as well as for the deactivated (after AST) sol–gel prepared coatings, a first--order transmission line was used, $R_\Omega(Q_{out}(R_p(Q_{in})))$ (the inscription according to ref. 46), where R_Ω is the ohmic resistance of the electrolyte, R_p is the pore resistance of the coating layer facing the electrolyte, while Q_{out} and Q_{in} are constant phase elements (CPE) related to the capacitance of the coating outer and inner active surfaces, respectively.

For the deactivated thermally prepared anode, a second-order transmission line EEC was applied to describe the anode impedance behavior at 0.50 V. This EEC indicates the separable EIS response of distinctive inner coating layers; hence the circuit inscription is $R_\Omega(Q_{out}(R_p(Q_{in}(R'(Q_{in}'))))))$. R' is the resistance closely related to the pore resistance of the inner layer to which Q_{in} relates, while Q_{in}' is the CPE related to the capacitance of an inner layer placed deeper in the bulk of the coating.

The values of the parameters of the EEC elements are given in Table I. The high R_p values obtained for both the sol–gel and thermally prepared active coatings indicate that the active surface of the inner coating is hardly accessible to the electrolyte. A lower R_p value was obtained for the thermally prepared anode, which supports the conclusion that this anode consisted of wider pores and cracks than the sol–gel prepared one, as concluded from the CV and polarization measurements. Considering Q_{out} as the capacitance of the surface layer (n values close to 1), values of 7.6 and 5.4 mF cm^{-2} (per apparent surface area) were calculated for the sol–gel and thermally prepared anode, respectively. These values agree with those registered by CV for t_{AST} = 0 h (Fig. 20), which confirms the difficult electrolyte penetration to the active surface of the inner coating due to narrow pores of high R_p values. The sweep rate applied in the CV was rather high for the active sites of the inner coating to be seen in the CV response. This is also seen from Y_0 values of Q_{in} for active coatings, with n values close to 0.5, which indicate that Q_{in} represents not only the capacitive behavior, but also the frequency-dependent diffusion processes in coating pores. Mobility of the ions of different radii is different, and can be considerably slower within the pores than

in electrolyte bulk.[47] This results in the formation of an instant electric micro--field within the pores, which slows down the faster ions and speeds up the slower ones. At higher frequencies, the ions cannot follow the fast alternation of potential, which is seen as a diffusion limitation represented by the values of the n parameter close to 0.5.[48] The value of $Y_{0,in}$ of the Q_{in} element indicates that almost one-third of the active sites of the coating are hardly accessible to the electrolyte (if $Y_{0,in}$ is compared to $Y_{0,in} + Y_{0,out}$).

TABLE I. Parameters of the equivalent electrical circuits used for the description of the impedance behavior of the investigated anodes at 0.50 V_{SCE} in 1.0 mol dm^{-3} $HClO_4$ (Reprinted with permission of Elsevier)[36]

Parameter		Anode prepared by:			
		Sol-gel procedure		Thermal decomposition	
		Before AST	After AST	Before AST	After AST
R_Ω / Ω		1.3	1.2	1.2	1.4
R_p / Ω		994	3.9	926	5.2
R' / Ω		–	–	–	360
Q_{out}	$Y_{0,out}$ / $k\Omega^{-1}$ s^n	6.0	0.12	4.2	0.095
	n	0.93	0.78	0.93	0.80
Q_{in}	$Y_{0,in}$ / $k\Omega^{-1}$ s^n	2.6	1.6	1.7	1.3
	N	0.66	0.86	0.44	0.83
Q_{in}'	$Y_{0,in}$' / $k\Omega^{-1}$ s^n	–	–	–	1.2
	n	–	–	–	0.40
ΣC / mF cm^{-2}		11.0	2.2	7.5	3.3

As the result of deactivation, R_p and Y_0 of Q_{out} considerably decreased for both the sol–gel and thermally prepared coating (Table I), which is the conesquence of the dissolution of Ru species from the outer coating surface. The coating porosity increased but the number of active sites decreased. A lower Y_0 value of Q_{out} was obtained after AST for the thermally prepared anode, which implies a faster dissolution of Ru species from outer coating surface than in the case of the sol–gel prepared anode. For the sol–gel prepared anode, the Y_0 of Q_{in} decreased, also for the same reason, but the decrease in the Y_0 value of Q_{in} for the thermally prepared anode was negligible. In addition, the n values of Q_{in} increased after AST for both the sol–gel and thermally prepared anode, which supports the fact that the electrolyte penetrates to the inner active sites of deactivated coatings easier than to those of the active coatings. It can be seen that the sum of the Y_0 values of Q_{in} and Q_{in}' for the deactivated thermally prepared coating (2.5 $k\Omega^{-1}$ s^n) is considerably higher than the Y_0 value of Q_{in} for the deactivated sol–gel prepared coating (1.6 $k\Omega^{-1}$ s^n), despite the lower Y_0 value of Q_{in} for the thermally prepared coating before AST (1.7 $k\Omega^{-1}$ s^n). This shows that Ru dissolution prevails at the inner active surface of the sol–gel prepared coating, which is not the case for the thermally prepared coating. As a consequence, a conside-

rably greater number of active sites remain on the inner active surface of the thermally prepared coating than on the inner active surface of the sol–gel prepared coating. This is also seen from the values of the overall coating capacitance, ΣC, given in Table I. The overall capacitance was calculated as the sum of the Y_0 values of Q_{out}, Q_{in} and Q_{in}', since these elements are in parallel. A larger ΣC value was obtained for the sol–gel prepared coating before AST than for the thermally prepared one, but the reverse was obtained after AST.

The resistance registered after AST for the thermally prepared anode, being the sum of R_p and R' (365 Ω), was considerably greater than the R_p of the sol–gel prepared anode (3.5 Ω), although the thermally prepared anode consisted of wider pores and cracks. This increased resistance could only be due to an insulating TiO_2 layer growing in the coating/substrate interphase.

6.4.2. Pore resistance and charge transfer resistance during deactivation

The impedance behavior of active coatings at 1.25 V (Figs. 22 and 23) is described through the simple EEC $R_\Omega(R_{ct}Q)$, where R_{ct} is the charge transfer resistance and Q is the CPE related to the coating resistance. As the active sites from the coating surface dissolve during AST, the EEC should be transformed into $R_\Omega(R_pQ_{out})(R_{ct,in}Q_{in})$. The physical meanings assigned to the EEC elements are based on the assumption that charge transfer at the deactivated anodes occurs mostly at the inner active sites, since the active sites disappeared from the outer surface during deactivation. Boodts and coworkers used a similar EEC to simulate the behavior of deactivated oxide coatings of different composition.[9,18]

The changes in R_p, R_{ct} (*i.e.*, $R_{ct,in}$) and the coating capacitance of both the sol–gel and thermally prepared anode during AST are given in Fig. 25. The coating capacitance was calculated with Q_{out} and Q_{in} in series. The changes in the coating capacitance are similar to the changes seen in Fig. 20. Since R_p does not depend on the anode potential, the R_p value for the active coating was taken from the EIS measurements at 0.50 V (Table I).

The R_{ct} value for the thermally prepared anode is higher than the value obtained for the sol–gel prepared anode, which indicates a higher activity of the latter. In the AST period below 29.7 h, R_{ct} and R_p considerably decreased. As the surface active sites dissolved, the pores and cracks became wider and a larger number of active sites from the inner active surface are exposed to the electrolyte. The charge transfer resistance is $R_{ct,in}$, owing to the effect recognized in Section 3.3 as the "opening of the inner coating structure". Once the inner active sites are opened for electrolyte penetration, they begin to dissolve, which results in the increase in R_{ct} and R_p for the AST period between 29.7 and 30.1 h. In the AST period between 30.1 and 31.1 h, the opening of the subsequent inner active surface, placed deeper into the bulk of the coating, is seen for sol–gel prepared anode as an additional decrease and subsequent increase in R_{ct}, while R_p continu-

ously increases. This effect was not seen for the thermally prepared anode. The significantly greater R_{ct} value after AST (31.1 h) was caused by the increasing content of TiO_2 in the coating/substrate interphase of this anode during AST.

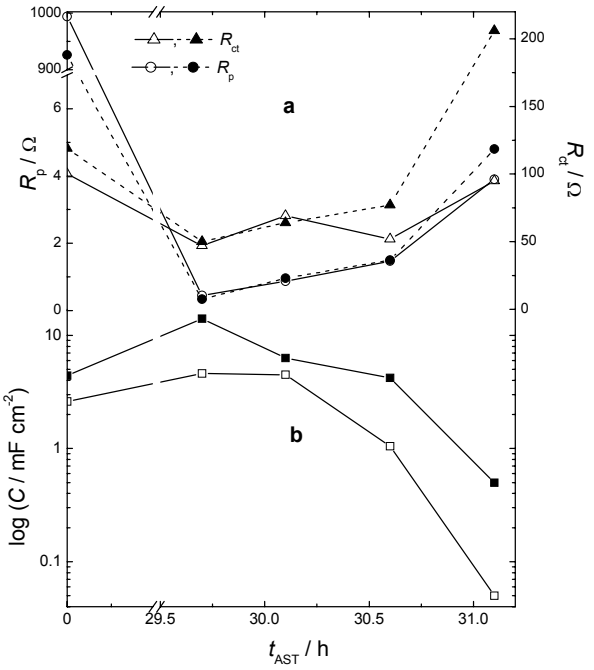

Fig. 25. The change in the pore resistance, R_p, charge-transfer resistance, R_{ct}, (a) and coating capacitance, C, (b) during AST for RuO_2–TiO_2/Ti anodes prepared by the sol–gel procedure and thermal decomposition. Empty symbols: sol–gel procedure, solid symbols: thermal decomposition. (Reprinted with permission of Elsevier).[36]

The obtained results show that the first stage in the deactivation mechanism for both the sol–gel and thermally prepared anode was Ru dissolution from the surface layer of the coating. In the case of the thermally prepared anode, the parallel progressive oxidation of the Ti substrate occurred in the subsequent stage, which additionally enlarged the insulating TiO_2 layer in the coating/substrate interphase. For the sol–gel prepared anode, this parallel process was less pronounced. This difference could explain the fact that the sol–gel prepared anode lasted longer in NaCl electrolysis, as was registered earlier, especially when thick coatings are considered.[23,28]

6.5. The stability of the ternary RuO_2–TiO_2–IrO_2 coating

The stability to ATA can be improved by the addition of IrO_2, which is believed to be more stable against dissolution during simultaneous vigorous oxygen evolution.[17] For this reason, commercial activated titanium anodes, available for cathodic protection purposes contain iridium oxide in small amounts, in addition to ruthenium and titanium oxide. Particularly, a good activity of ATA in seawater is important for their application in cathodic protection. The results of accelerated stability test performed in seawater on a ternary and a binary coating are shown

in Fig. 26, as the time dependence of the anode potential at a constant current density. Since IrO_2 is more stable during the simultaneous evolution of oxygen and chlorine, the durability of the ternary coating was longer than that of the binary coating. A tentative explanation for considerably larger stability of the ternary coating could be as follows. The reactions of RuO_2 dissolution and oxygen evolution proceed in parallel.[11] The mechanism for RuO_2 dissolution could be:

$$RuO_2 + H_2O \rightarrow RuO_2{-}OH + H^+ + e^- \quad (5)$$

$$RuO_2{-}OH \rightleftharpoons RuO_3 + H^+ + e^- \quad (6)$$

$$RuO_3 + H_2O \rightleftharpoons RuO_3{-}OH + H^+ + e^- \quad (7)$$

$$RuO_3{-}OH \rightleftharpoons RuO_4 + H^+ + e^- \quad (8)$$

while for the oxygen evolution reaction, the proposed mechanism[11] suggests that Steps (7) and (8) should be replaced by:

$$2RuO_3 \rightleftharpoons 2RuO_2 + O_2 \quad (9)$$

The Steps (5) and (6) are the same for the two mechanisms, with the formation of $RuO_2{-}OH$, Step (5), as the rate-determining step. The species in the subsequent Steps (7)–(9) decompose giving either oxygen or RuO_4, which is soluble in acid solutions. However, when IrO_2 is present in the coating, oxygen evolution occurs mainly at the IrO_2 active sites. This hinders the decomposition reactions on the RuO_2 active sites and considerably extends the service life of the coating.

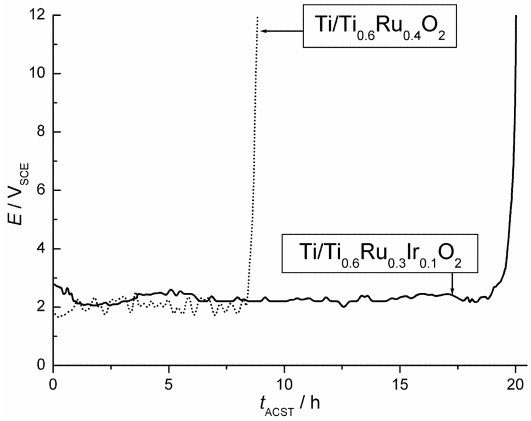

Fig. 26. Time dependences of the potential of the sol–gel anodes with ternary and binary coating during the accelerated stability test in seawater at a current density of 0.60 A cm^{-2}.[37]

CONCLUSIONS

The results obtained in investigations of activated titanium anodes prepared by the inorganic sol–gel procedure are reviewed. Microscopic investigations of oxide sols and coatings showed that the ageing time of the sols defines the coating morphology and, consequently, the electrochemical behavior of a coating. Better electrochemical characteristics, including anode stability in electrolysis, was registered for a combination of small RuO_2 and large TiO_2 particles.

Anode deactivation is manifested by an increased coating resistance and by a deceased electrochemically active surface area. The increase in the coating resistance is more pronounced for traditional thermally prepared coatings, while sol–gel prepared coatings show a more pronounced decrease in the electrochemically active surface area. The initial increase in coating resistance is caused by the dissolution of Ru species from the coating surface facing the electrolyte, which restricts the coating activity to the active sites of the inner coating. For the thermally prepared anode, there is additional increase in coating resistance due to the enlargement of an insulating TiO_2-rich layer in the coating/substrate interphase. This enlargement is considerably less pronounced during the deactivation of sol–gel prepared anodes. Thus, the main cause for deactivation of a thermally prepared anode is a TiO_2 layer in the interphase, while the dissolution of a Ru species prevails in the deactivation process of sol–gel prepared coatings, which makes the coating surface layers enriched in TiO_2.

Investigations of a ternary, sol–gel prepared RuO_2–TiO_2–IrO_2 coating on titanium showed that it has similar basic electrochemical properties as a binary RuO_2–TiO_2 coating. However, the results of an accelerated stability test on the binary and ternary coating showed that the ternary coating was considerably more stable during exploitation in seawater than the binary one. This is the consequence of the greater stability of IrO_2 under vigorous oxygen and chlorine evolution in comparison to RuO_2. This fact makes the ternary coating a better candidate as the anode in real applications for cathodic protection.

Acknowledgements. Financial support from the Ministry of Science and Technological Development of the Republic of Serbia under Grant No. 14062 is acknowledged. Thanks are due to the colleagues which significantly participated in the research work: Slobodan K. Milonjić ("Vinča" Institute of Nuclear Sciences, University of Belgrade, Serbia), Aleksandar B. Dekanski (ICTM–IEC, University of Belgrade, Serbia), Vesna B. Mišković-Stanković (Faculty of Technology and Metallurgy, University of Belgrade, Serbia) and Radoslav T. Atanasoski (Present address: 3M Company, St. Paul, MN, USA).

И З В О Д

ТИТАНСКЕ АНОДЕ АКТИВИРАНЕ ОКСИДНОМ ПРЕВЛАКОМ ДОБИЈЕНОМ СОЛ–ГЕЛ ПОСТУПКОМ

ВЛАДИМИР В. ПАНИЋ[1] и БРАНИСЛАВ Ж. НИКОЛИЋ[2]

[1]ИХТМ – Центар за електрохемију, Његошева 12, Београд и [2]Технолошко–металуршки факултет, Карнегијева 4, Београд

У раду је дат је преглед својстава активираних титанских анода, RuO_2–TiO_2/Ti и RuO_2–TiO_2–IrO_2/Ti, добијених сол–гел поступком од неорганских оксидних солова. RuO_2 и TiO_2 солови добијени су форсираном хидролизом одговарајућих хлорида метала у киселој средини. Морфологија добијених солова испитивана је трансмисионом електронском микроскопијом. Хемијски сатав RuO_2 сола испитиван је дифракцијом х-зрака и термогравиметријском анализом. Механизам губитка електрокаталитичке активности RuO_2–TiO_2/Ti анода испитиван је праћењем промена електрохемијских својстава аноде у реакцијама издвајања хло-

ра и кисеоника, као и на потенцијалу отвореног кола, током деградације аноде. Ове електрохемијске карактеристике аноде испитиване су методама цикличне волтаметрије, спектроскопије електрохемијске импеданције и поларизационим мерењима. Промене у електрохемијским својствима аноде добијене сол–гел поступком поређене су са променама које су регистроване за RuO_2–TiO_2/Ti аноду добијену традиционалним поступком термичке разградње хлорида метала. На основу ових испитивања произилази да је основни узрок губитка електрокаталитичке активности аноде добијене сол–гел поступком електрохемијско растварање RuO_2, док је узрок деградације аноде добијене термичком разградњом раст непроводног TiO_2 слоја у међуфази превлака/титанска подлога. Резултати убрзаног теста стабилности RuO_2–TiO_2/Ti и RuO_2–TiO_2–IrO_2/Ti аноде показују да је тројна превлака знатно стабилнија од двојне, због веће стабилности оксида иридијума у поређењу са оксидом рутенијума.

(Примљено 3. марта, ревидирано 2. септембра 2008)

REFERENCES

1. S. Trasatti, in *Interfacial Electrochemistry – Theory, Experiment and Applications*, A. Wieckowski, (Ed.), Marcel Dekker Inc., New York, 1999, p. 769.
2. B. Conway, *Electrochemical Supercapacitors – Scientific Fundamentals and Technological Applications*, Plenum Publishers, New York, 1999, p. .
3. T. Jow, J. Zheng, *J. Electrochem. Soc.* **145** (1998) 49
4. M. Ramani, B. Haran, R. White, B. Popov, *J. Electrochem. Soc.* **148** (2001) A374
5. [5]D. Rolison, P. Hagans, K. Swider, J. Long, *Langmuir* **15** (1999) 774
6. [6]K.-W. Park, B.-K. Kwon, J.-H. Choi, In-Su Park, Y.-M. Kim, Y.-E. Sung, *J. Power Sources* **109** (2002) 439
7. S. Trasatti, *Electrochim. Acta* **36** (1991) 225
8. V. A. Alves, L. A. Silva, J. F. C. Boodts, *J. Appl. Electrochem.* **28** (1998) 899
9. L. M**.** Da Silva, L. A. De Faria, J. F. C. Boodts, *J. Electroanal. Chem.* **532** (2002) 141
10. V. M. Jovanović, A. Dekanski, P. Despotov, B. Ž. Nikolić, R. T. Atanasoski, *J. Electroanal. Chem.* **339** (1992) 147
11. Lj. M. Gajić-Krstajić, T. Lj. Trišović, N. V. Krstajić, *Corr. Sci.* **46** (2004) 65
12. G. N. Martelli, R. Ornelas, G. Faita, *Electrochim. Acta* **39** (1994) 1551
13. F. Beck, *Electrochim. Acta* **34** (1992) 811
14. J.-M. Hu, J.-Q. Zhang, C.-N. Cao, *Inter. J. Hydrogen Ener*. **29** (2004) 791
15. V. V. Gorodetskii, V. A. Neburchilov, V. I. Alyab'eva, *Russ. J. Electrochem*. **41** (2005) 1111
16. T.-X. Cai, H. Chen, H. Ju, L.-N. Lu, *Corr. Potection* **27** (2006) 522
17. M. G. Pavlović, A. B. Dekanski, *J. Solid State Electrochem*. **1** (1997) 208
18. T. A. F. Lassali, J. F. C. Boodts, L. O. S. Bulhões, *J. Appl. Electrochem.* 30 (2000) 625
19. V. V. Panić, A. B. Dekanski, S. K. Milonjić, V. B. Mišković-Stanković, B. Ž. Nikolić, *Russ. J. Electrochem.* **42** (2006) 1173
20. V. V. Panić, A. B. Dekanski, S. K. Milonjić, V. B. Mišković-Stanković, B. Ž. Nikolić, *J. Serb. Chem. Soc.* **71** (2006) 1173
21. V. V. Panić, T. R. Vidaković, A. B. Dekanski, V. B. Mišković-Stanković, B. Ž. Nikolić, *J. Electroanal. Chem*. **609** (2007) 120
22. V. Panić, T. Vidaković, S. Gojković, A. Dekanski, S. Milonjić, B. Nikolić, *Electrochim. Acta* **48** (2003) 3805
23. V. Panić, A. Dekanski, S. Milonjić, R. Atanasoski, B. Nikolić, *Electrochim. Acta* **46** (2000) 415

24. V. Panić, A. Dekanski, S. Milonjić, R. Atanasoski, B. Nikolić, *Mater. Sci. Forum* **352** (2000) 117
25. J. P. Zheng, T. R. Jow, *J. Electrochem. Soc.* **142** (1995) L6
26. J. Zhang, D. Jiang, B. Chen, J. Zhu, L. Jiang, H. Fang, *J. Electrochem. Soc.* **148** (2001) A1362
27. V**.** Panić, A. Dekanski, G. Wang, M. Fedoroff, S. Milonjić, B. Nikolić, *J. Colloid Interface Sci*. **263** (2003) 68
28. V. Panić, A. Dekanski, S. Milonjić, R. Atanasoski, B. Nikolić, *Colloids Surfaces A* **157** (1999) 269
29. A. De Battisti, G. Lodi, M. Cappadonia, G. Battaglin, R. Kötz, *J. Electrochem. Soc.* **136** (1989) 2596
30. M. Guglielmi, P. Colombo, V. Rigoto, G. Battaglin, A. Boscolo-Boscoletto, A. De Battisti, *J. Electrochem. Soc.* **139** (1992) 1655
31. K. Komeyama, S. Shohji, S. Onoue, K. Hishimura, K. Zahikozawa, Y. Takasu, *J. Electrochem. Soc.* **140** (1993) 1034
32. F. I. Mattos-Costa, P. de Lima-Neto, S. A. S. Machado, L. A. Avaca, *Electrochim. Acta* **44** (1998) 1515
33. S. Ardizzone, S. Trasatti, *Adv. Colloid Interface Sci.* **64** (1996) 173
34. V. V. Panić, A. B. Dekanski, V. B. Mišković-Stanković, S. K. Milonjić, B. Ž. Nikolić, *J. Serb. Chem. Soc.* **68** (2003) 979
35. L. M. Da Silva, L. A. De Faria, J. F. C. Boodts, *Electrochim. Acta* **47** (2001) 395
36. V. Panić, A. Dekanski, V. B. Mišković-Stanković, S. Milonjić, B. Nikolić, *J. Electroanal. Chem*. **579** (2005) 67
37. V. V. Panić, B. Ž. Nikolić, *J. Serb. Chem. Soc*. **72** (2007) 1393
38. L. A. De Faria, J. F. C. Boots, S. Trasatti, *Electrochim. Acta* **42** (1997) 3525
39. E. Matijević, M. Budnik, L. Meites, *J. Colloid Interface Sci.* **61** (1977) 352
40. F. I. Mattos-Costa, P. de Lima-Neto, S. A. S. Machado, L. A. Avaca, *Electrochim. Acta* **44** (1998) 1515
41. V. Panić, A. Dekanski, V. Mišković-Stanković, B. Nikolić, S. Milonjić, *Mater. Manufacturing Proc.* **20** (2005) 89
42. Y. Murakami, T. Kondo, Y. Shimoda, H. Kaji, K. Yahikozawa, Y. Takasu, *J. Alloys Comp.* **239** (1996) 111
43. Y. Takasu, T. Arikawa, K. Yanase, X.-G. Zhang, Y. Murakami, *J. Alloys Comp.* **261** (1997) 172
44. V. Panić, A. Dekanski, S. Milonjić, R. Atanasoski, B. Nikolić, *J. Serb. Chem. Soc*. **65** (2000) 649
45. Yu. Chizmadzev, Yu. Chirkov, in *Comprehensive Threatise of Electrochemistry Vol. 6,* E. Yeager, J. Bockris, B. Conway, S. Sarangapani, (Eds.), Plenum press, New York, 1983, Ch. 5.
46. B. Boucamp, *Equivalent Circuit (EQUIVCRT.PAS) Users Manual*, University Twente, Enschede, the Netherlands, 1989
47. V. B. Mišković-Stanković, J. B. Zotović, Z. Kačarević-Popović, M. D. Maksimović, *Electrochim. Acta* **44** (1999) 4269
48. W. H. Mulder, J. H. Sluyters, T. Pajkossy, L. Nyikos, *J. Electroanal. Chem*. **285** (1990) 103.